Pergamon

PII: S0301-9322(96)00021-3

Int. J. Multiphase Flow Vol. 22, No. 4, pp. 651–665, 1996

0301-9322/96 $15.00 + 0.00

EXPERIMENTAL STUDY OF A TWO-PHASE BUBBLY FLOW IN A FLAT DUCT SYMMETRIC SUDDEN EXPANSION—PART 1: VISUALIZATION, PRESSURE AND VOID FRACTION

F. ALOUI and M. SOUHAR

LEMTA (CNRS URA-875)-ENSEM-INPL. 2, Avenue de la Forêt de Haye 54516, Vandœuvre-Lès-Nancy, France

(Received 20 December 1994; in revised form 14 March 1996)

Abstract—The present work involves an experimental study of bubble flow in a flat horizontal sudden expansion. This study consists of two parts which are interdependent and complementary. Here in the first part, the qualitative study by visualization shows that the bubble flow changes from a dissymetric configuration to a symmetric configuration beyond a certain volumetric quality x. The quantitative study involves evolutions of the pressure and the void fraction downstream of the singularity for a quasi-symmetric bubble flow. Copyright © 1996 Elsevier Science Ltd.

Key Words: two-phase gas–liquid flow, bubbly flow, plane sudden expansion, visualization of bubble flow, pressure, void fraction

1. INTRODUCTION

Nowadays two-phase gas–liquid systems in industrial processes occupy an important place and pose many problems to the engineer during conception and dimensioning of installations concerned by such systems. Precise knowledge of two-phase flows, either a better understanding of certain phenomena (void migration, blocking, coalescence, etc.) or control of industrial operations (pressure drop, heat and mass transfer), is of basic interest.

Transport circuits in two-phase industrial installations are mainly composed of various singularities which provoke significant modifications of the flow. Among these singularities, the case of a sudden expansion corresponds to a common situation in practice.

In single-phase flow, this type of singularity is largely treated in literature both theoretically and experimentally. In the case of two-phase flow, most studies were carried out in an axisymmetric sudden expansion configuration. The major works carried out on this type of singularity in bubble flow involve singular pressure drop and global void fraction. For the singular pressure drop, several global models were proposed (Richardson 1958; Lottes 1961; Chisholm & Sutherland 1969; Wadle 1989). These models present significant deviations from experiments (Suleman 1990; Aloui 1994). On a local basis, one can refer to the theoretical works of Bel Fdhila (1991) and Bel Fdhila & Simonin (1992), which led to the development of a calculation code named "Melodif" which predicted local void fraction and the different average and turbulent quantities of the continuous phase in axisymmetric sudden expansion.

In the case of the sudden expansion of a flat duct, encountered in plate heat exchangers for example, bubble flow remains quite unknown both theoretically and experimentally. In order to contribute to understanding of the reorganisation of this two-phase flow downstream of the singularity, a qualitative study was carried out by visualizing the flow at several volumetric qualities x as well as a study of the evolution of the pressure and the void fraction downstream of the expansion.

We can also note the great attempt undertaken actually in multidimensional modeling and finding closure laws, as can be seen for example in two-fluid models, Lahey (1995). There of, the sudden expansion case constitutes a reliable test for this model. So as to minimize the number of measurements points, we have chosen a particular configuration of sudden expansion (figure 1),

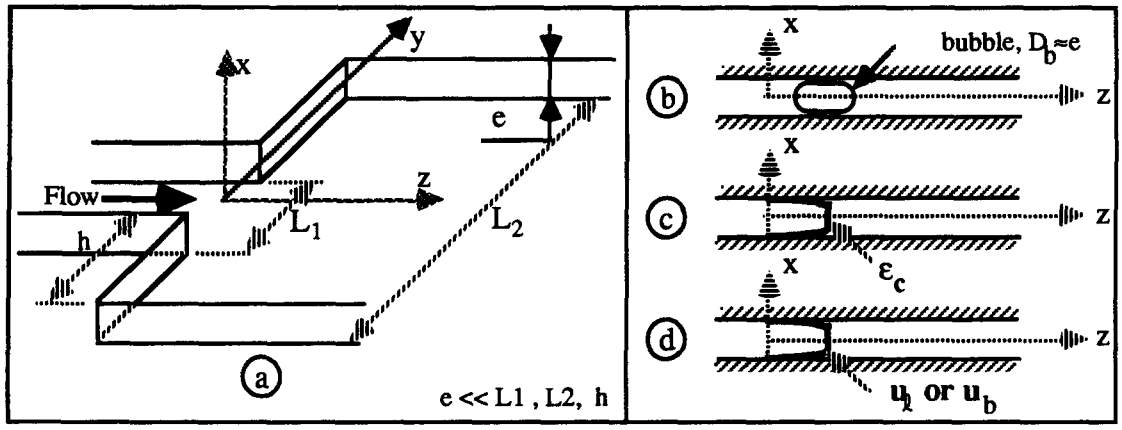

Figure 1. The particular geometry investigated and the void fraction and phase velocities expected.

and bubble sizes close to the thickness of the flow "e" (figure 1(b)). Such choice allows almost flat profiles of void fraction and both phases velocities (figure 1(c) and (d)). Therefore, most of our measurements have been carried out in $z = 0$ plane. Besides, as far as modeling is concerned, this particular configuration will certainly lead to equations more obvious than in the tridimensional case.

2. EXPERIMENTAL AND MEASURING DEVICE

2.1. Experimental device

Experimental arrangement, as shown in figure 2, is used for the study of the effects of the sudden expansion on the "two-dimensional" flows. This set up is composed basically of two circuits. A "closed" liquid circuit regulated at 20 ± 0.5°C and an "open" gas circuit. Both circuits feed a test section with rectangular cross sections of 44 × 55 mm² and 100 × 5 mm² upstream and downstream of the expansion, respectively. The liquid and gas flowrates were measured by a diaphram flowmeter and an STH-Hastings mass flowmeter (series HFC203), respectively.

The experimental test section was made using transparent plexiglass with the aim of carrying out direct visualization of the flow and local measurements (pressure, void fraction, axial velocity and granulometry). This test section, of 460 mm long with a rectangular cross section 100 × 5 mm² downstream of the singularity, ensures a plane and "two dimensional flow". The length of the duct before the expansion is 125 mm. This length has been chosen particularly short to give a good initial condition (at $\zeta = 0$). The step height h is 28 mm and the ratio of the cross sections upstream and downstream of the expansion is $\sigma = 0.444$. The upper wall of the test section (figure 3), composed of a sliding plate made of transparent plexiglass, is equipped with two openings provided for housing the interchangeable measuring blocks. The first block describes the flow upstream of the expansion (at $z = 30$ mm) up to half way of the test section, and the second takes over from there up to $z = 402$ mm downstream of the expansion (figure 3). With the aid of a probe support located on the measuring block which allows a transversal displacement (along y) and a rack-and-pinion system which guides the sliding plate longitudinally, it is possible to reach everywhere points in the expansion. This sliding plate having openings for the measuring blocks (pressure and velocity), is interchangeable with another flat transparent plate intended exclusively for the visualization of single-phase flow and bubbly flow. Figure 4 shows a longitudinal and three dimensional section of the test section without the upper plate, and a detail of the injection system.

The pressure measuring block has nine pressure tappings connected to a differential pressure probe with variable range. The measuring blocks of void fraction, average and fluctuating local liquid and gas velocity, and granulometry of bubbles are each equipped with a micrometric displacement device in the transversal direction of the flow. Local measurements of the void fraction, axial velocity and granulometry of bubbles were made with an RBI double optical fibre

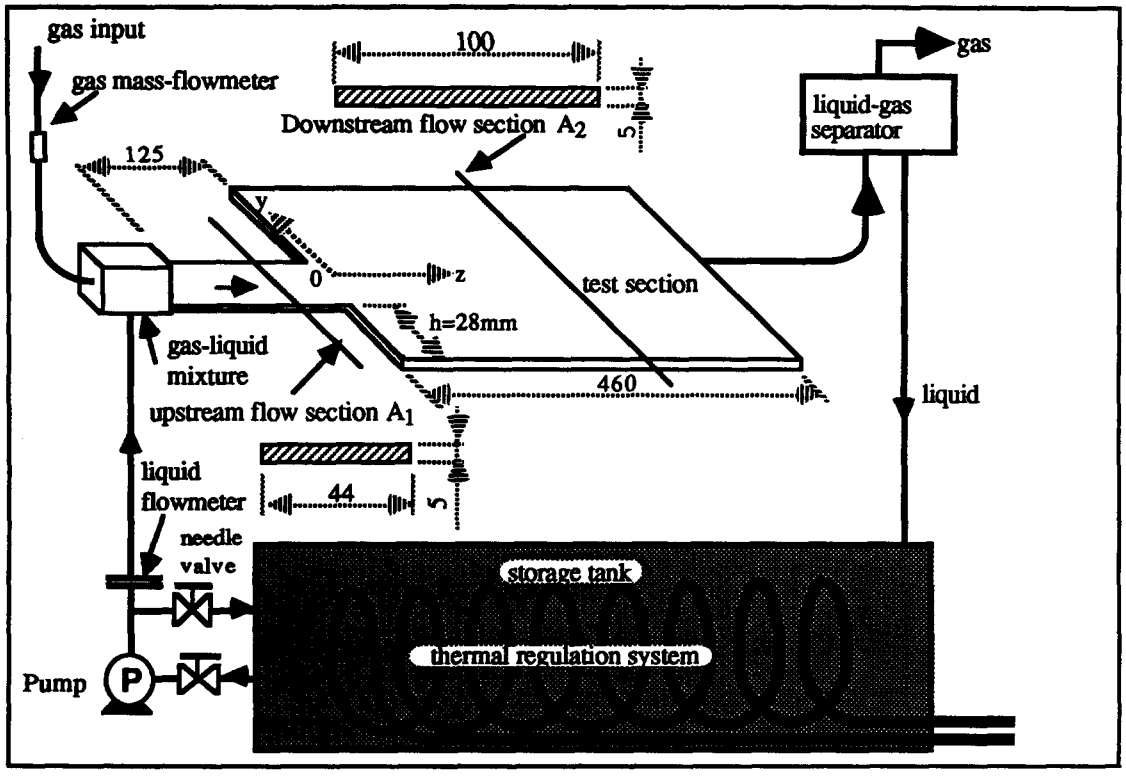

Figure 2. Schematic diagram of the experimental apparatus (dimensions in mm).

probe (the size of the tip is about 40 μm). This consists of two single optical probes separated by a distance of 1.10 mm. The measurement of the average and fluctuating axial velocity of the liquid phase was made by hot film probe. The anemometric system is composed of an electronic control (DISA 55MO1) and a 1210–1220 W hot film ($\phi \approx 40$ μm). The signals obtained for the different measured quantities were processed on a UNIX HP9360 station. For each flow rate, a fine grid consistent of many points of measurement spread uniformly downstream of the sudden expansion was used.

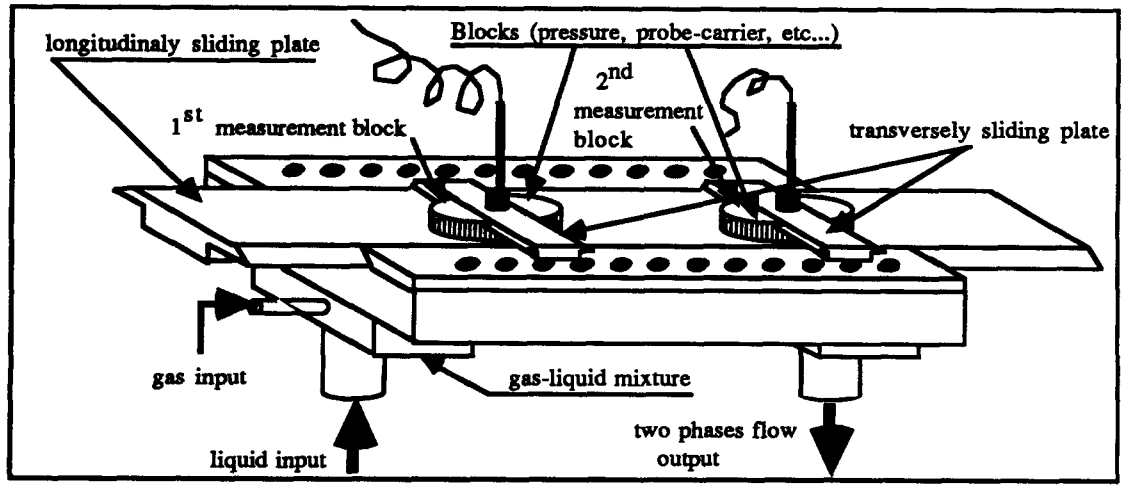

Figure 3. Three dimensional view of the horizontal test section.

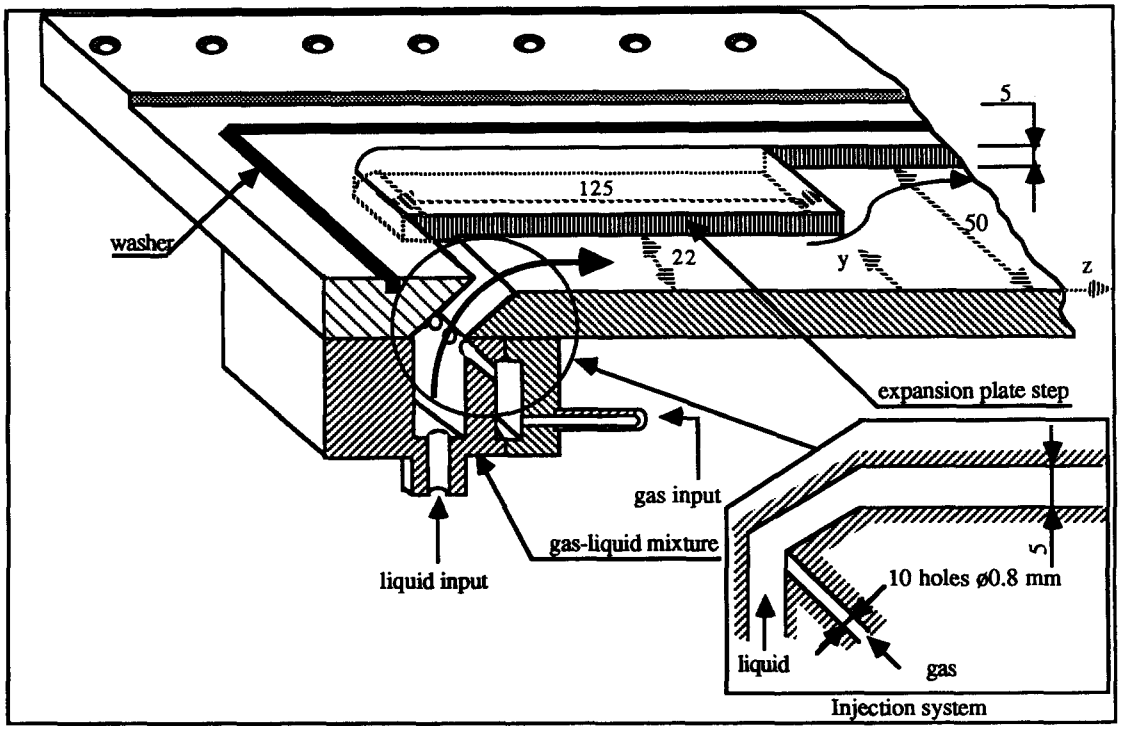

Figure 4. Three dimensional cutting of the test section without upper plate and detail of the injection system (dimensions in mm).

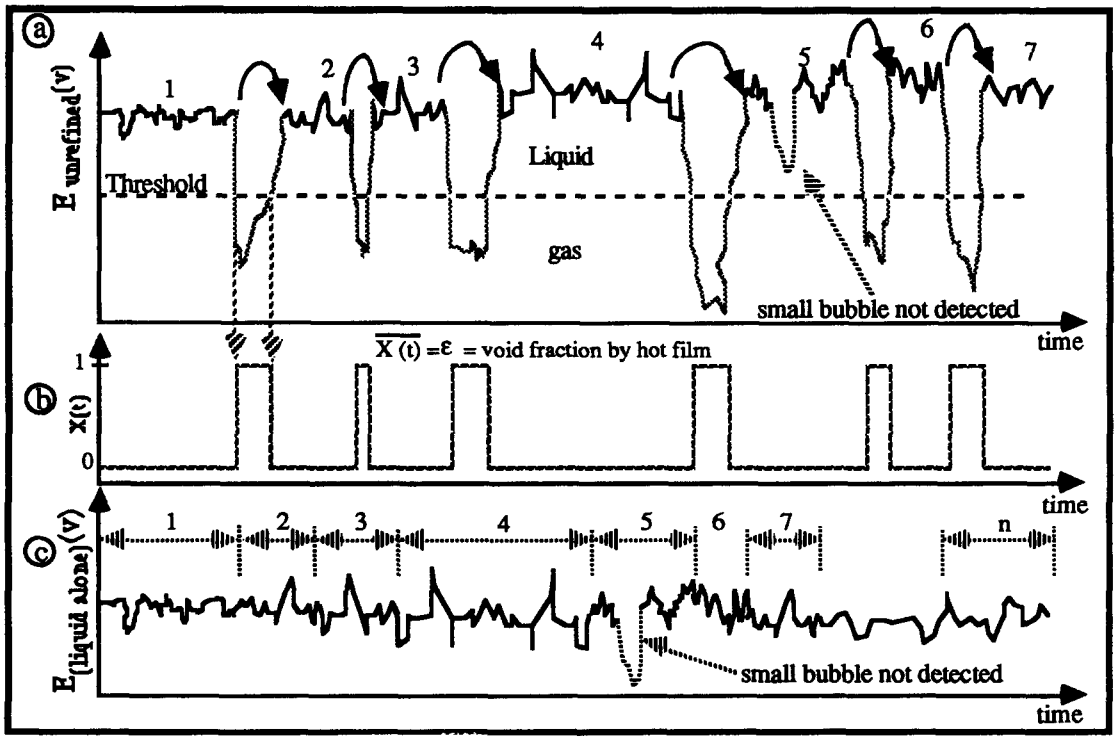

Figure 5. The extractory principle of the liquid phase signal from the unrefined two-phase flow signal delivered by the hot film.

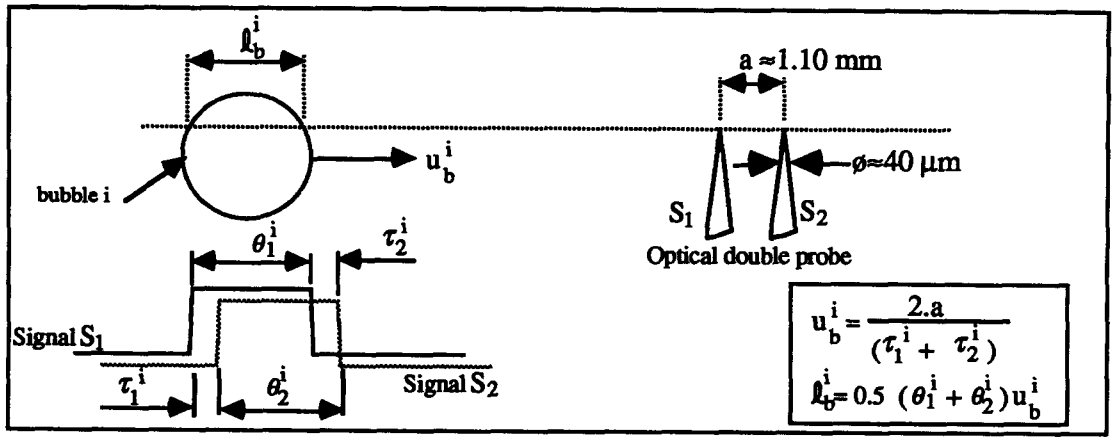

Figure 6. Calculation method of the axial velocity and the bubble sizes by the optical double probe.

2.2. Procedure of numerical processing of signals

2.2.1. Hot film probe signals. The axial velocity of the liquid was measured by a hot film probe. The untreated voltage signal obtained at the exit of the amplifier (figure 5(a)) is filtered at a given threshold, then transformed into a signal of liquid only by an automatic elimination of all bubble passages and by joining together the remaining portions of signals (figure 5(c)). The calibration curve is used to transform the voltage signal into a velocity signal. The threshold is chosen such that the local void fraction obtained by the phase indicator function of the hot film probe (figure 5(b)) is close to that measured previously with the optical probe. This method is not rigorous since the signal of the liquid only may still contain some small bubbles, and the joints could introduce steps in the signal. However, this procedure does not affect the average value of the axial velocity, but can affect the fluctuating quantities slightly or significantly depending on the flow conditions. Also, the latter represent only an order of magnitude of the turbulence quantities of the liquid phase. Later, the classical method based on the histograms treatment (Delhaye 1968, 1969), has been used and leads to the same results.

It is well known that changes in the flow direction cannot be detected by using of the hot film anemometry. Further, we assume that the direction of the liquid phase velocities u_L, in a big vortex ($1 < \zeta \leqslant 7{,}5$), is the same than bubble velocities u_b direction. This latter being correctly determined by double optical probes. In the small vortex ($0 \leqslant \zeta \leqslant 1$) which contains few bubbles, the direction of u_L have been taken the same that the measurements by LDA in single liquid flow in axisymmetric sudden expansion (Aloui 1994).

2.2.2. Signals obtained from the optical double probe. The different magnitudes related to the gaseous phase are extracted from the two signals delivered by the optical double probe. The acquisition of these signals at each point of the flow was carried out for a sufficiently long period (about 200 s). The sampling frequency was fixed at 65 KHz in order to give a precision of about 4% on bubble velocity. The optical signal delivered by each of the two probes are in the form of random square waves. The thresholds are defined for these square waves then transformed into a logical signal with an amplitude equal 1 or 0 V corresponding to the gaseous and the liquid phases, respectively. The local void fraction is determined from the average of the two void fractions obtained from the probes. The axial velocity of the bubbles is obtained from the two logical signals and the distance of 1.10 mm between the two optical fibres as shown in figure 6.

Bubble flow is very chaotic and possess random bubble diameters. This leads to several cases of the two logical signals as shown in figure 7. Only the last case (figure 7(d)) is retained; it consists of studying only *bubbles with size greater than or equal to the distance separating the sensitive parts of the double optical probe*. This procedure has the advantage of measuring the bubble velocity correctly but it has the disadvantage of losing much of the information and excluding all small sized bubbles. In this case (figure 7(d)), the axial velocity u_b^i of the ith bubble as well as the "cutting

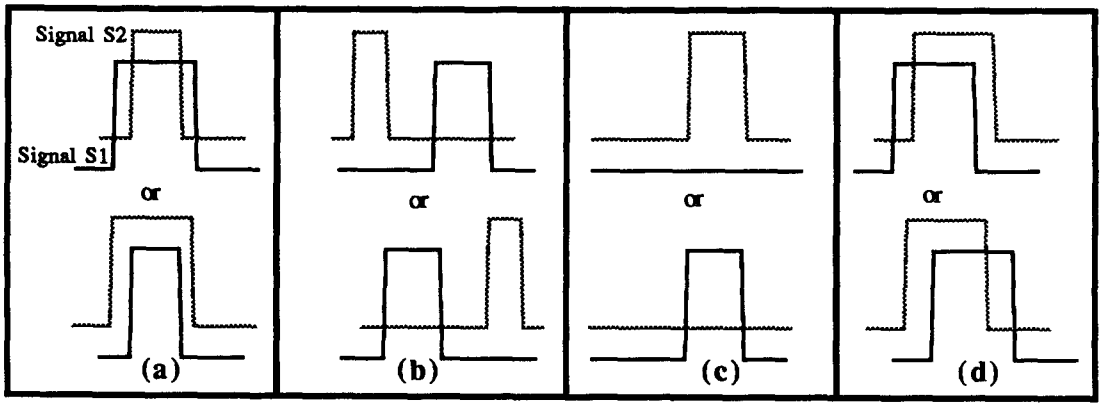

Figure 7. The different cases of the bubbles crossing the optical double probe.

length" l_b^i were measured (figure 6). The whole data concerning u_b^i and l_b^i were used to construct signals ith bubble, having the axial velocity u_b^i and the cutting length l_b^i. The average and fluctuating values were calculated using the latter signals by using the probability density established for each signal. The local average bubble diameter is obtained by using the following relation (Belakhovsky 1966; Galaup 1975; Herringe & David 1976; and Clark & Turton 1988):

$$D = 1.5\bar{l}_b \quad \text{where} \quad \bar{l}_b = \int_0^\infty l_b P(l_b)\, dl_b$$

$P(l_b)$ represents the probability distribution function of the lengths l_b. The example of $P(l_b)$ given in figure 8 shows an important dispersion of the "cutting length" l_b. This means that we have big flat bubbles sized up to 12 mm in the flow. However, the probability of these bubbles remains small.

In order to control the measurement of the average velocity $\bar{u}_b$ by this "statistical" procedure, a cross-correlation method of the two logical signals was used. The direction of the flow and the velocity were obtained directly by the optimal time τ_{opt} of the temporal cross-correlation. The calculation algorithm of the different magnitudes related to the dispersed phase was programmed in U.P.A., a language specific to L.M.S. which, itself, makes use of the sub-programmes in language "C" in order to accelerate computing.

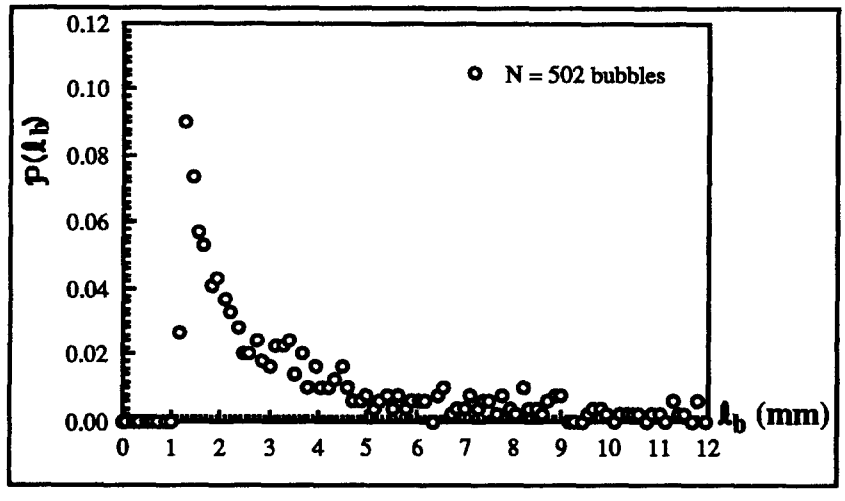

Figure 8. Probability distribution function of the "cutting lengths" at $\zeta = 0$, $y = 0$, $U_{LSI} = 3.2$ m/s and $x = 20.83\%$.

3. RESULTS AND DISCUSSIONS

3.1. *Visualization of the flow*

The bubble flow in the sudden expansion was visualized by using a Reflex camera (1/30 to 1/1000th of a second). A photograph of the flow was taken at variable shutter speeds for a superficial liquid velocity of $U_{LSI} = 7$ m/s and a variable volumetric quality x. At very low gas flowrate, the flow, which is almost similar to a single-phase flow, is entirely asymmetrical downstream of the singularity as illustrated in the photograph of figure 9(a). It is observed that at the exit from the singularity, the flow bends towards the left (with regards to the direction of the arrow) to hit the side wall then deviated towards the right to hit other wall. This situation described recently by Gagnon *et al.* (1993) and Aloui (1994) in turbulent single-phase flow led, in this work, to highlighting regions of vortices at both sides of the axis of the expansion with different sizes. At the left side of the singularity, the vortex has a dimensionless length of $\zeta_{left} \approx 6 \pm 0.5$. This vortex is similar to the one obtained in axisymmetrical flow (Aloui 1994). Whereas on right side, the vortex of dimensionless length of $\zeta_{right} \approx 9 \pm 0.5$, gives a line that separates it from the rest of the flow. The latter curves towards the center of the flow then moves from it and gets reattached

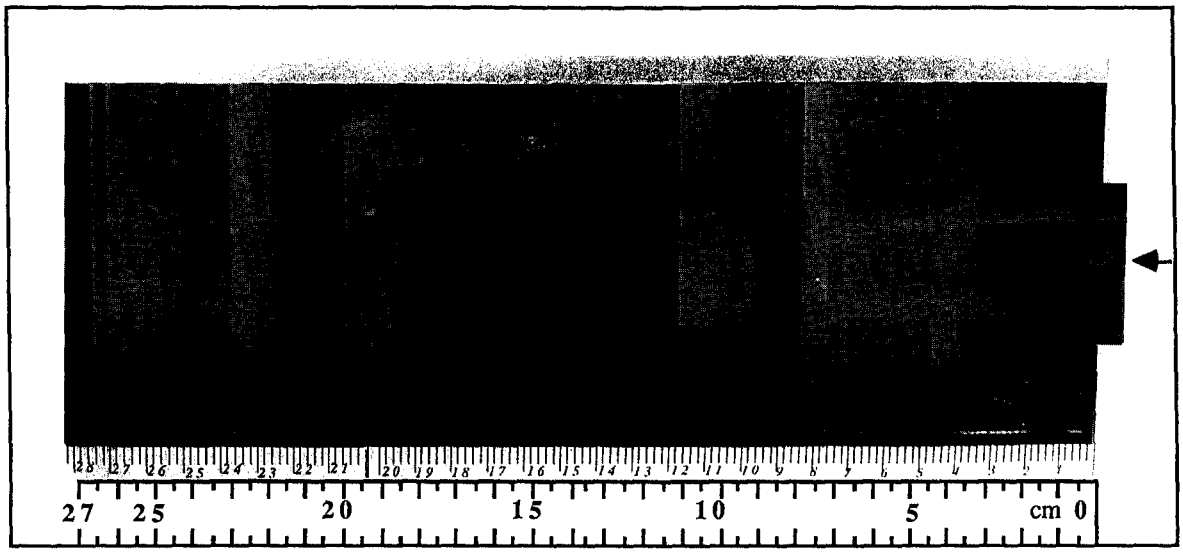

(a)

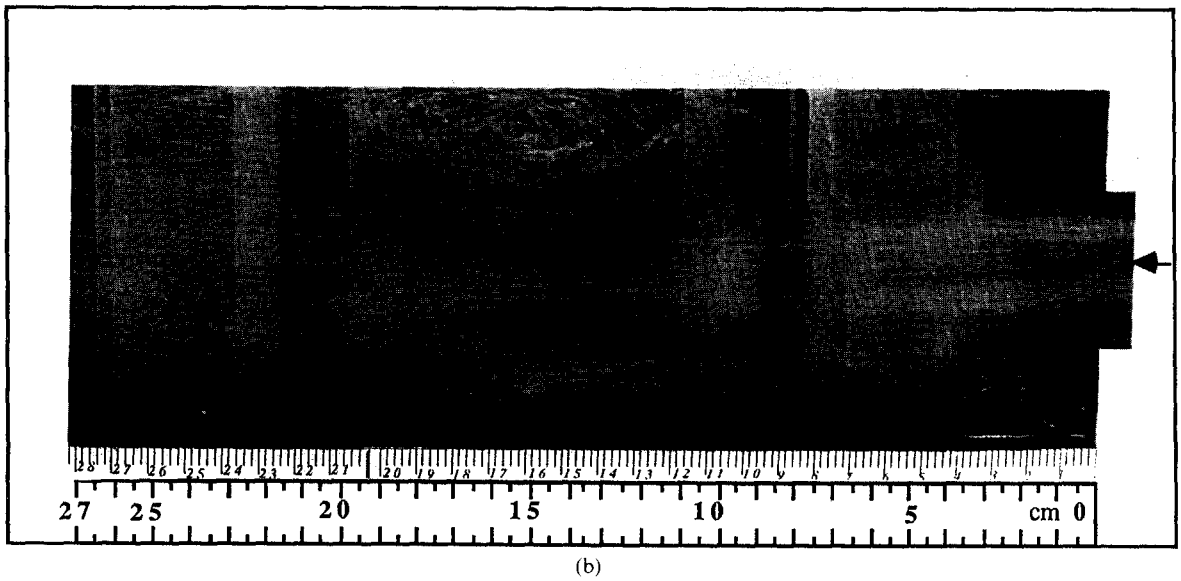

(b)

Figure 9. Downstream flow visualization in the sudden expansion. (a) $U_{LSI} = 7$ m/s and $x = 1\%$; (b) $U_{LSI} = 7$ m/s and $x = 14.4\%$.

Table 1. Different couples of liquid and gas superficial velocities used in the experiment

U_{LSI} (m/s)	U_{GSI} (m/s)	x (%)
3.20	0.842	20.83
3.20	1.166	26.70
4.80	1.526	24.12
4.80	2.259	32.00

to the wall (at $\zeta_{right} \approx 9 \pm 0.5$). The flow is strongly unstationary inside the vortices and presents small vorticities which unite and disintegrate with time. A small unstationary vortex is formed after the reattachment point of the recirculating flow region. Beyond this last vortex, the flow returns to a quasi-symmetric one. It should be noted that this dissymmetry is not varying in time and sometimes located at the left and at other times at the right.

For a given liquid flowrate when the gas flowrate is increased, it is possible to obtain a practically symmetrical flow as illustrated by the photograph in figure 9(b). The examination of the different liquid and gas flowrates shows that the bubbly flow is symmetric for volumetric quality upper to 10%. Evidently, this conclusion is only valuable for our particular sudden expansion.

Henceforth, only symmetrical bubble flow will be studied. For that, four couples of liquid and gas flowrates shown in the table 1, were examined. An example of the visualization of these regimes is given in figure 10. This example clearly shows the quasi-symmetry of the flow. The vortex regions are practically stable and of equal sizes. So, the horizontal and "two dimensional" configuration allows therefore a better view of the recirculating regions compared to an axisymmetric configuration, and is easier to model. For these reasons, a complete experimental study of this case was proposed in order to constitute a data bank. These data will serve to test local models in the short-term.

3.2. *Evolution of the pressure*

In view of the symmetry of the flow in the sudden expansion, the static pressure was measured by numerical acquisition of signals in one half downstream of the sudden expansion ($0 < y \leqslant 50$ mm, $0 \leqslant z \leqslant 400$ mm). These signals were recorded for a sufficiently long period then processed to obtain the average pressure $\bar{p}$. The variation of the pressure for all the flowrates already mentioned is reproducible. Results of measurement are presented in 3D and contour plots form. For example, figure 11(a) and (b) gives this pressure distribution for the superficial velocities

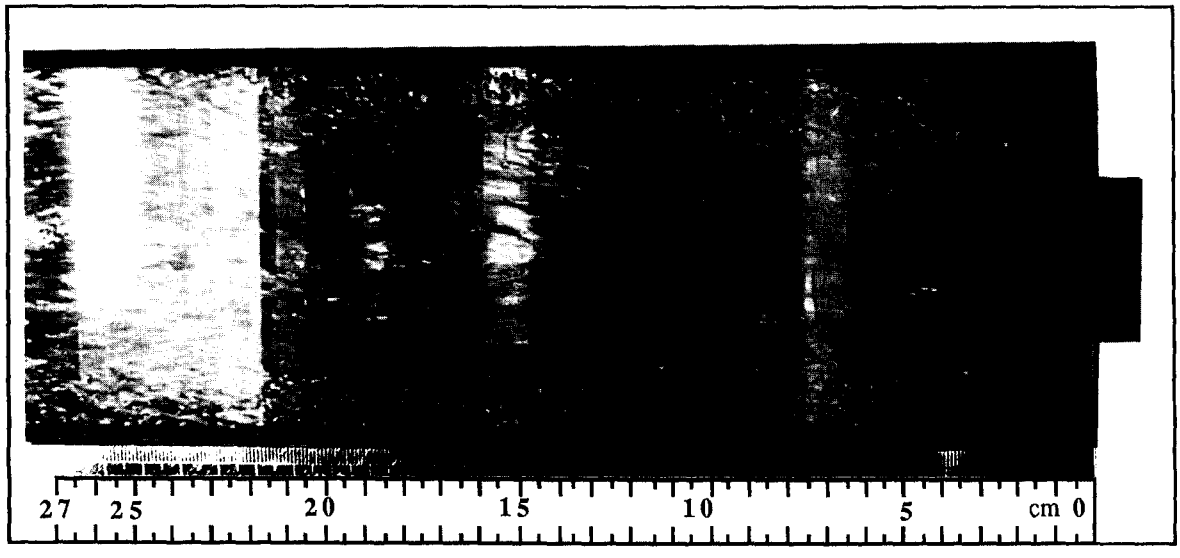

Figure 10. Downstream flow visualization in the sudden expansion ($U_{LSI} = 3.2$ m/s and $x = 27.7$)%.

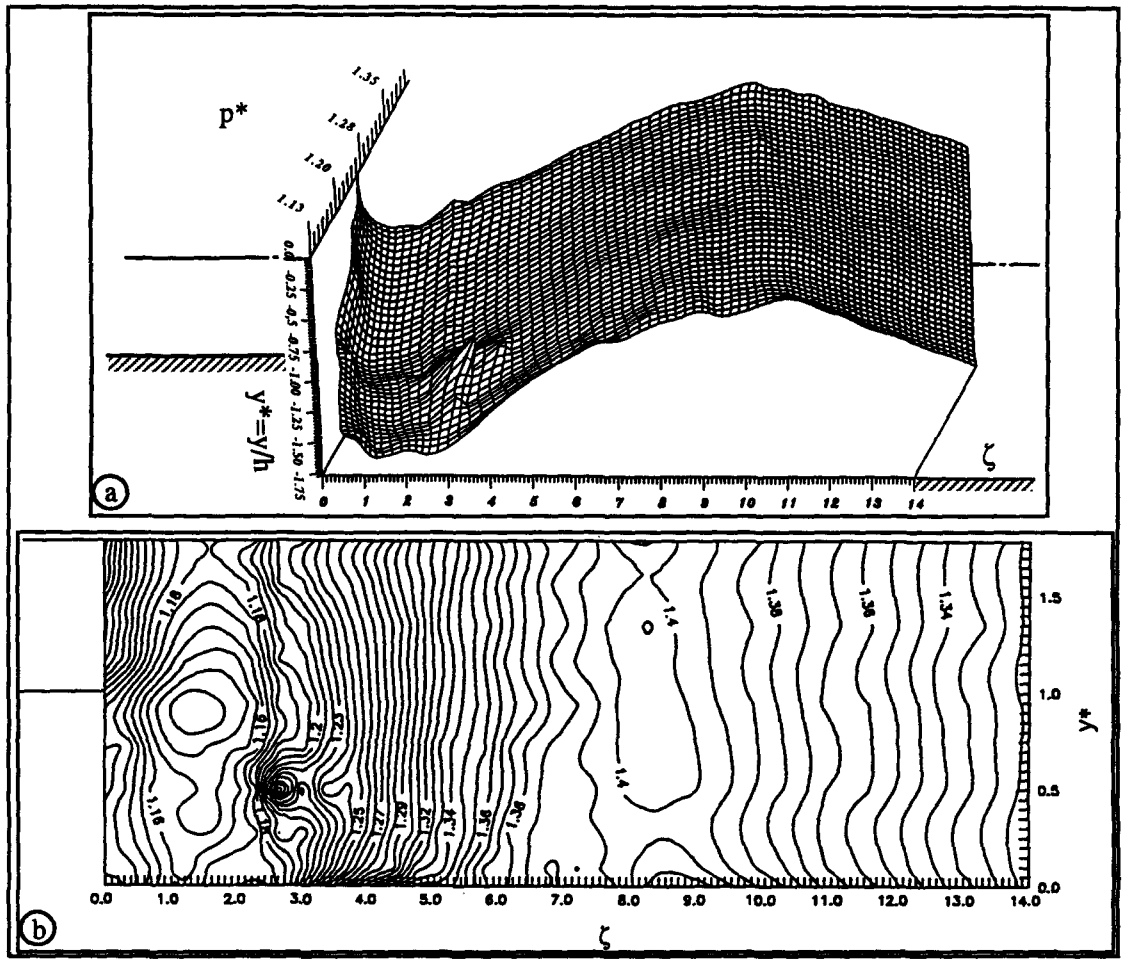

Figure 11. Pressure distribution under sudden expansion for $U_{LSI} = 3.2$ m/s and $x = 20.83\%$. (a) 3D view; (b) contour plots.

$U_{LSI} = 3.2$ m/s and $U_{GSI} = 0.842$ m/s. In these figures, the average pressure is normalized in the following manner:

$$p^* = \frac{\bar{p} - p_{atm}}{\frac{1}{2}\rho_L U_{LSI}^2}$$

where p_{atm} is the atmospheric pressure and U_{LSI} the superficial velocity of the liquid in the upstream section of the expansion.

In these evolutions, the pressure decreases along z progressively up to a minimum then, increases to reach a maximum and lastly decreases linearly with the dimensionless length ζ. These results are similar to those obtained by Suleman (1990), Aloui *et al.* (1993) and Aloui (1994) in axisymmetric sudden expansion with vertical and horizontal configurations. It should be noted however that in the axisymmetrical case (Suleman 1990), the maximum pressure is reached at about $\zeta = 10$–11, whereas in this case, this maximum is located in the neighbourhood of $\zeta = 7$–8. Beyond this last maximum, the decrease of the pressure is more pronounced due to the shear stress which is relatively high in this case (Aloui 1994).

The results of pressure measurements along the centre line ($y = 0$) far away upstream and

downstream from the singularity for $U_{LSI} = 3.2$ m/s and $U_{GSI} = 0.842$ m/s are shown in figure 12(a) and (b). From these measurements, we can deduce:

$$-\left(\frac{\partial p}{\partial z}\right)_{\text{upstream}} = -28050 \quad \text{S.I.} \quad \text{and} \quad -\left(\frac{\partial p}{\partial z}\right)_{\text{downstream}} = -3750 \quad \text{S.I.}$$

Along the center line ($y = 0$) upstream and far away downstream, we can suppose that the forces on bubbles can be reduced only to pressure forces ($\approx$ buoyancy) and drag forces. The lift forces can be neglected because of small rotational of the flow in these zones. In such conditions, we have:

$$\frac{4}{3}\rho_G \pi R^3 \frac{\mathrm{d}\mathbf{u}_b}{\mathrm{d}t} = \int_{\text{Surf.Bubble}} -p\mathbf{n}\,\mathrm{d}s + \textbf{Drag force} \approx \mathbf{0}$$

by using Gauss theorem:

$$\int_S \bar{\bar{T}}\mathbf{n}\,\mathrm{d}s = \int_v \mathrm{div}(\bar{\bar{T}})\,\mathrm{d}v, \quad \bar{\bar{T}} = -p\bar{\bar{I}},$$

one obtains:

$$0 = \frac{4}{3}\pi R^3\left(-\frac{\partial p}{\partial z}\right) - C_D\frac{1}{2}\rho_L|v_r|v_r\pi R^2$$

where R is the radius of bubble, v_r the relative velocity ($u_b - u_L$) and C_D the drag coefficient. Assuming that C_D remains the same than for a sphere in infinite medium $C_D \approx 0.44$ and $R \approx 3$ mm, we obtain:

$$(v_r)_{\text{upstream}} \approx 0.70 \text{ m/s} \quad \text{and} \quad (v_r)_{\text{downstream}} \approx 0.24 \text{ m/s}.$$

We shall see in the following (Part 2) that these values are of the same magnitude than those measured.

3.3. Evolution of the local and average void fraction

Measurements of void fraction at every point downstream of the sudden expansion was carried out using a double optical probe. An example of void fraction profile in inlet sudden expansion ($\zeta = -0.35$), is given in figure 13, and constitute an interesting data of the initial boundary conditions for numerical simulation.

The distribution of the local void fraction downstream of the sudden expansion is presented in 3D and contour plots form. For example, figure 14(a) and (b) show the evolution of the dispersed phase in the expansion. Immediately at exit from the expansion ($z = 2$ mm after), a maximum of

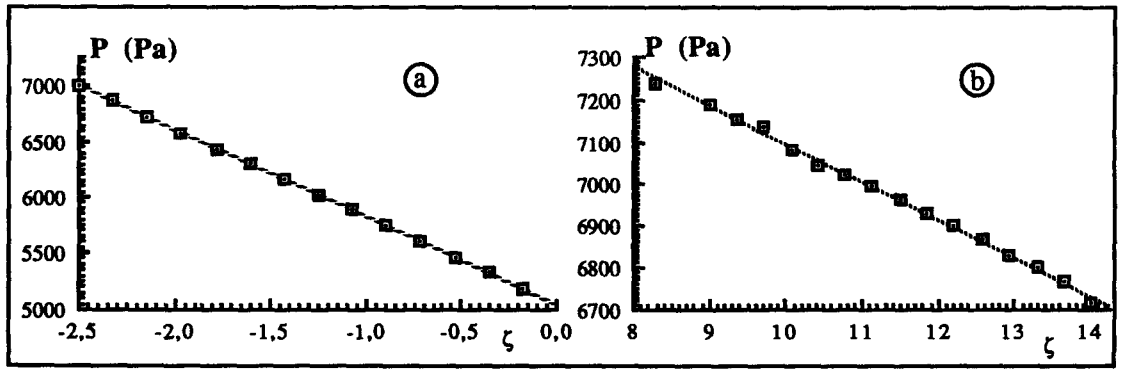

Figure 12. Pressure loss for $U_{LSI} = 3.2$ m/s and $x = 20.83\%$. (a) Upstream of the singularity; (b) downstream of the singularity of $\zeta > 8$.

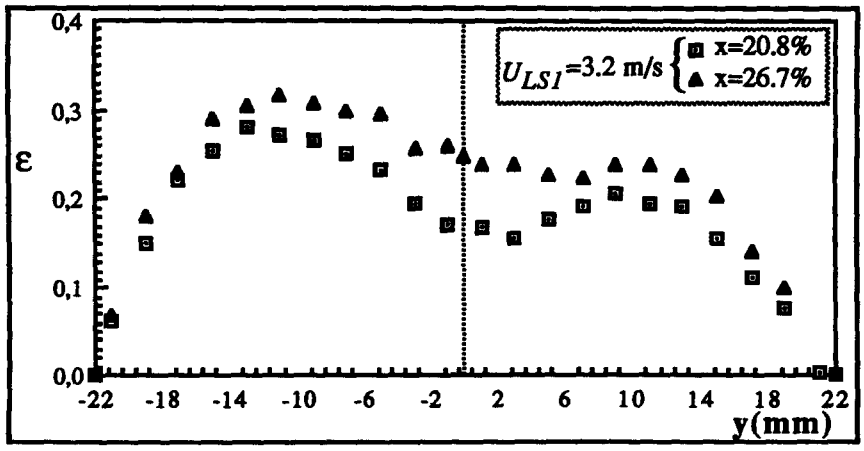

Figure 13. Void fraction profiles in the upstream of the sudden expansion; $\zeta = -0.35$.

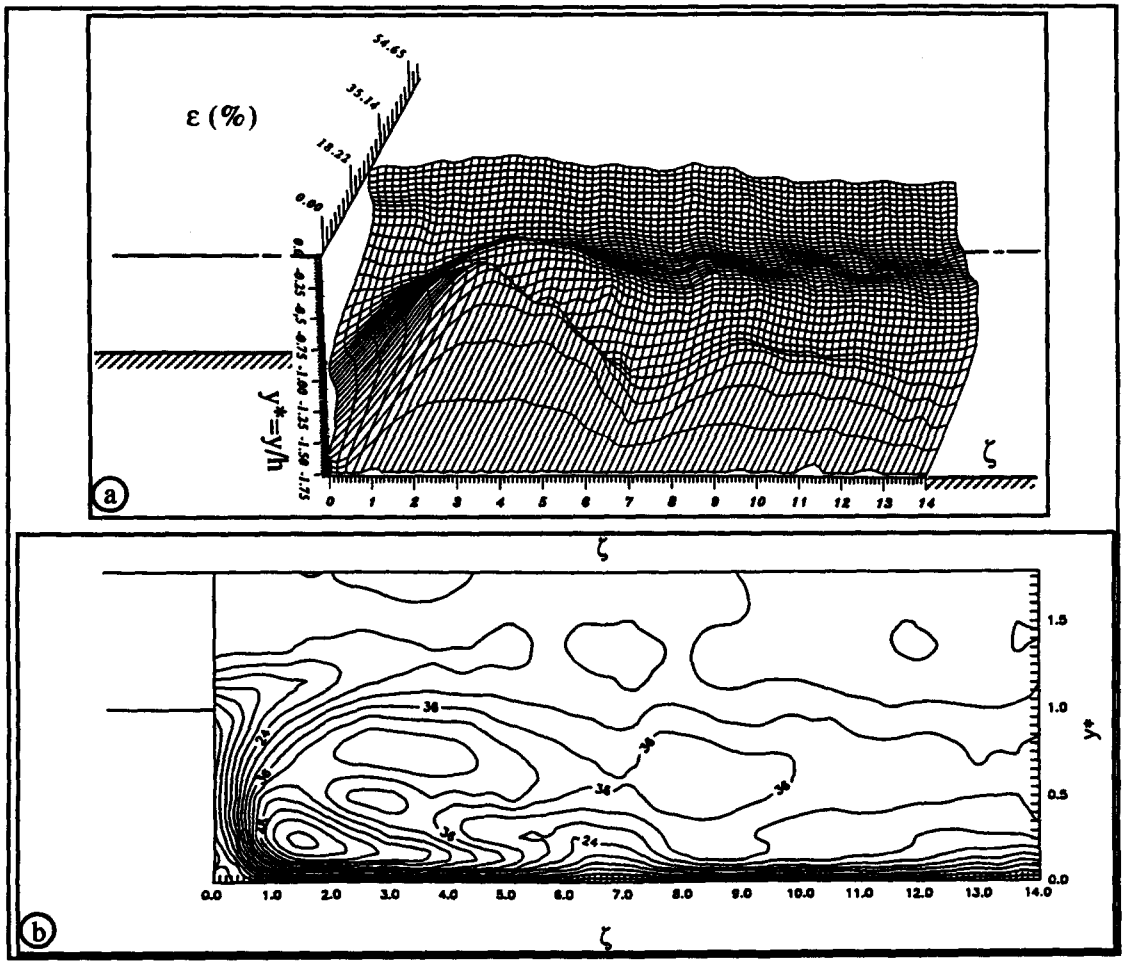

Figure 14. Void fraction distribution under sudden expansion $U_{SL1} = 3.2$ m/s and $x = 20.83\%$. (a) 3D view; (b) contour plots.

void fraction is observed around the axis of the test section and a very low void fraction close to the step, implying that a few bubbles come to be housed down within the step. In the big vortex, the void fraction measured seems to be the maximum observed in the whole test section. The bubbles captured in the recirculating region keep rotating in closed trajectories. Along these stream lines, bubble velocity progressively changes from a negative value near the wall to reach a maximum positive value at the center of the expansion. The profile defining this trajectory passes inevitably by a zero value. The point corresponding to the latter is referred to as "vortex center". At this point, the bubbles are practically stationary and as such, either the optical fibre or the hot film probe gives a maximum void fraction. It is observed that the presence of bubbles is low in the vicinity of the reattachment point at $\zeta = 7$–8. In this region, the bubbles have the tendency of either moving in the direction of the main flow or going back to be trapped in the recirculating zone by following closed trajectories. In figure 14(a), it is observed that there is a relative minimum for each profile at constant ζ. These minima seem to be located on the jet line. Beyond the reattachment point, the distribution of the void fraction begins to be reorganised and later becomes similar to the one obtained upstream of the expansion.

The variation of the local void fraction along the lateral wall downstream of the singularity (at $y = 47$ mm) is given by figure 15. In this region, the void fraction is practically zero up to $\zeta = 0.5$ (region of single-phase flow). Beyond $\zeta = 0.5$, the void fraction increases progressively to reach high values which are likely to produce coalescence of bubbles; then it decreases to reach a minimum at $6.5 \leqslant \zeta \leqslant 7.5$ (reattachment point). As from $\zeta \leqslant 7.5$, the flow tends towards a reorganisation of establishment of the regime.

Figure 16 shows the evolution of the average void fraction $\langle \epsilon \rangle$ with respect to each section and as a function of the dimensionless distance ζ. As in the case of the axisymmetrical sudden expansion (Suleman 1990; Aloui 1994), the average void fraction is low up to the inlet of the singularity. This average increases progressively to reach a maximum located at $\zeta = 2$, then it decreases to reach a constant plateau beyond $\zeta = 10$. The ratio of the average void fraction measured downstream to that upstream at the inlet level (just at $\zeta = 0.07$) is close to its limiting value σ.

At the inlet of the singularity ($\zeta = 0.357$), the average void fractions ϵ_1 are satisfactory comparable with existing correlations (table 2). As for the average downstream void fraction ϵ_2, it is of the same order as ϵ_1 ($\pm 10\%$), which is different from the axisymmetrical case (table 2).

The results obtained in Part 2 can be used to determine the region of principal flow. In this flow, the average of the ratio of the void fraction ($\langle \epsilon(\zeta) \rangle / \langle \epsilon(\zeta = 0) \rangle$) relative to each section outside the recirculating region to the one at the inlet of the expansion varies as shown by figure 17. The average void fraction increases progressively starting from the inlet into the singularity up to maximum at about $\zeta = 3.8$, then begins to decrease up to the reattachment point. Beyond the latter,

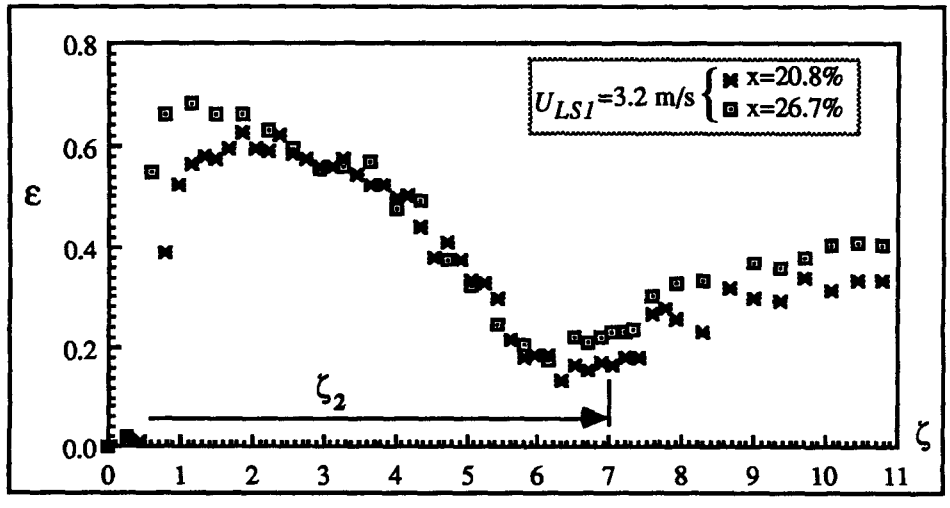

Figure 15. Local void fraction of 3 mm from lateral wall downstream of the sudden expansion.

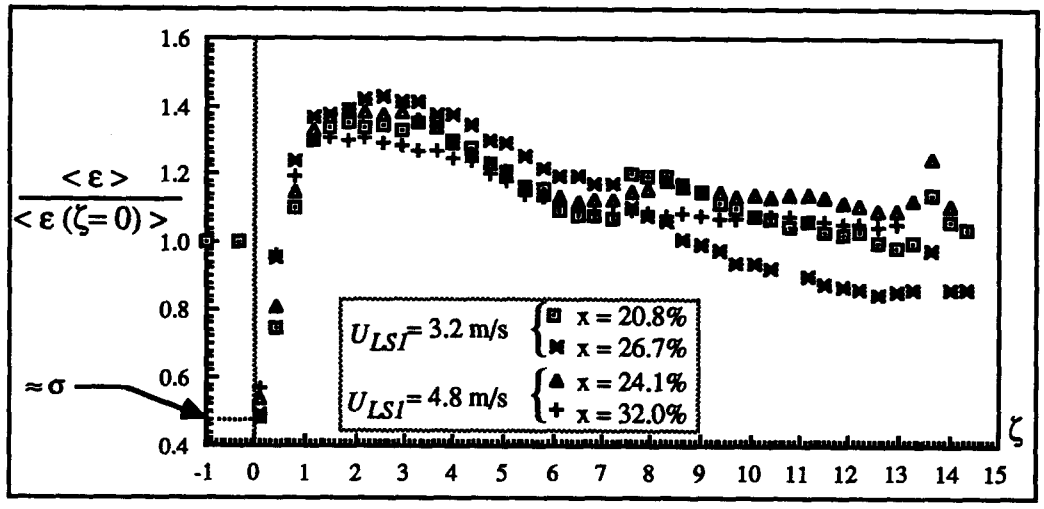

Figure 16. Average void fraction distribution downstream of the sudden expansion.

Table 2. Comparison of different experimental slopes with those obtained by other authors

	Suleman (1990) experimental axisymmetric	Petrick & Swanson (1958)	Aloui (1994) experimental axisymmetric	Present work
$\frac{\langle \epsilon_1 \rangle}{x}$	0.830	—	0.860	0.846
$\frac{\langle \epsilon_2 \rangle}{\langle \epsilon_1 \rangle}$	0.830	0.705	0.750	0.984

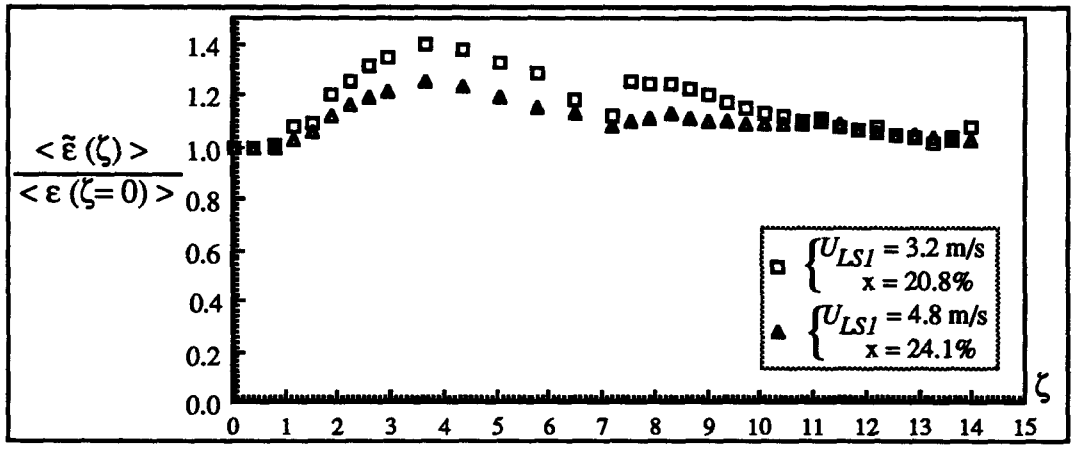

Figure 17. Average void fraction distribution in the principal flow downstream of the sudden expansion.

the recirculating region to the one at the inlet of the expansion varies as shown by figure 17. The average void fraction increases progressively starting from the inlet into the singularity up to maximum at about $\zeta = 3.8$, then begins to decrease up to the reattachment point. Beyond the latter, the variation of this ratio becomes very low and tends towards the value of 1 obtained at the inlet into the expansion.

4. CONCLUSION

This experimental study on bubble flow in a flat sudden expansion supplies results on visualization, pressure and void fraction. The results of visualization show that bubble flow is asymmetrical for low volumetric qualities and becomes practically symmetrical for void fractions above about 10%.

Pressure measurements show that the pressure remains almost constant in each section (ζ = constante), unlike what was obtained in asymmetrical single-phase flow. The evolution of the pressure along the expansion is similar to that obtained in axisymmetrical sudden expansion. In our case, the pressure gradient upstream and downstream are much higher than the vertical duct. Consequently, relative velocities are sure to be found.

The results of local void fraction downstream of the sudden expansion point out two regions in which the void fraction undergoes different variations. In the recirculation region, maximum void fraction is observed which corresponds to the center of the big vortex where bubble velocities are practically zero. The local void fraction decreases progressively when one moves far from the singularity along the axis of the expansion in the main flow. Beyond $\zeta = 8.5$ where the flow begins to be reestablished, the variation of the void reaction which is similar to the one upstream of the expansion remains the same. The average void fraction is low at the entrance into the expansion and increases progressively to reach a maximum at about $\zeta = 2$, and then decreases to a plateau value beyond $\zeta = 10$.

REFERENCES

Aloui, F., Azzoun L., Souhar, M. & Si Ahmed, E. K. 1993 Etude expérimentale d'un écoulement à bulles à travers un élargissement brusque bidimensional. *Premier Congrès de Mécanique (S.M.S.M), Actes*, pp. 209–217, Avril 1993—Rabat, Morocco.

Aloui, F. 1994 Etude des écoulements monophasiques et diphasiques dans les élargissements brusques axisymétrique et bidimensionnel. Thèse de Doctorat de l'INPL, Nancy, France.

Aloui, F. & Souhar, M. 1994 Etude de la chute de pression singulieagre dans les élargissements brusques en écoulement monophasique turbulent. *J. Appl. Math. Phys. (ZAMP)* **45,** 371–386.

Belakhovsky, M. 1966 Eléments d'une description statistique d'un écoulement diphasique—écoulement eau-air à bulles. C.E.N.-G., Note interne TT No. 226, Avril, France.

Bel Fdhila, R. 1991. Analyse expérimentale et modélisation d'un écoulement vertical à bulles dans un élargissement brusque. Thèse de Doctorat de l'INPT, Toulouse, France.

Bel Fdhila, R. & Simonin, O. 1992 Modélisation des écoulements turbulents à bulles: Application à un élargissment brusque en conduite verticale, EDF/LNH-Groupe Méca. Fluides Industrielles, ARD-AID no. E4404R, Chatou, France.

Chisholm, D. & Sutherland, L. A. 1969 Prediction of pressure gradients in pipeline systems during two-phase flow. *Proc. Inst. Mech. Engrs* **184,** 24–43.

Clark, N. N. & Turton, R. 1988 Chord length distributions related to bubble size distributions in multiphase flows. *Int. Multiphase Flow* **14,** 413–424.

Delhaye, J. M. 1968 Anemometry with hot film in two-phase flow. Measure of levels in presence of gas. *C.r. Acad. Sci. Paris* **266,** 370–373.

Delhaye, J. M. 1969 Hot-film anemometry in two-phase flow. *Eleventh Nat. ASME/AIChe Heat. Transfer Conf. Minneapolis* Aug. pp. 58–69.

Gagnon, Y., Giovannini, A. & Hebrard, P. 1993 Numerical simulation and physical analysis of high Reynolds number recirculating flows behind sudden expansions. *Physics of Fluids A* **5,** 2377–2389.

Galaup, J. P. 1975. Contribution à l'étude des méthodes de mesure en écoulement diphasique. Thèse de Docteur-Ingeénieur, Grenoble, France.

Herringe, R. A. & Davis, M. R. 1976 Structural development of gaz-liquid mixture flows. *J. Fluid Mech.* **73,** 97–123.

Lahey, R. T. Jr 1995 The CFD analysis of multidimensional phenomena in multiphase flow. *Proceeding of the Second International Conference of Multiphase Flow '95-Kyoto*, Vol. 3, pp. M02-1–M02-8.

Lottes, P. A. 1961. Expansion loss in two-phase flow. *Nuclear Science and Engineering* **9,** 26–31.

Petrick, M. & Swanson, B. S. 1959 Expansion and contraction of air-water mixture in vertical two-phase flow. *AIChE J.* **5,** 440–445.

Richardson, B. 1958 Some problems in horizontal two-phase flow, two-phase-component flow. Report ANL-5949.

Suleman, S. O. 1990 Contribution à l'étude d'un écoulement gaz–liquide dans un élargissement brusque. Thèse de Doctorat de l'INPL, Nancy, France.

Wadle, M. 1989 A new formula for the pressure recovery in abrupt diffusor. *Int. J. Multiphase Flow* **15,** 241–256.